JOURNAL OF GEOPHYSICAL RESEARCH, VOL. 106, NO. C2, PAGES 2815-2832, FEBRUARY 15, 2001

Baroclinic transport variability of the Antarctic Circumpolar Current south of Australia (WOCE repeat section SR3)

Stephen R. Rintoul and Serguei Sokolov

CSIRO Marine Research and Antarctic Cooperative Research Centre
Hobart, Tasmania, Australia

Abstract. Baroclinic transport variability of the Antarctic Circumpolar Current (ACC) near 140°E is estimated from six occupations of a repeat section occupied as part of the World Ocean Circulation Experiment (WOCE section SR3). The mean top-to-bottom volume transport is 147±10 Sv (mean ±1 standard deviation), relative to a deep reference level consistent with water mass properties and float trajectories. The location and transport of the main fronts of the ACC are relatively steady: the Subantarctic Front carries 105±7 Sv at a mean latitude between 51° and 52°S; the northern branch of the Polar Front carries 5±5 Sv to the east between 53° and 54°S; the southern Polar Front carries 24±3 Sv eastward at 59°S; and two cores of the southern ACC front at 62° and 64°S carry 18±3 and 11±3 Sv, respectively. The variability in net property transports is largely due to variability of currents north of the ACC, in particular, an outflow of 8±13 Sv of water from the Tasman Sea and a deep anticyclonic recirculation carrying 22±8 Sv in the Subantarctic Zone. Variability of net baroclinic volume transport is similar in magnitude to that measured at Drake Passage. In density layers, transport variability is small in deep layers, but significant (range of 4 to 16 Sv) in the Subantarctic Mode Water. Variability of eastward heat transport across SR3 is significant (range of 139°C Sv, or 0.57 x 10^{15} W, relative to 0°C) and large relative to meridional heat flux in the Southern Hemisphere subtropical gyres. Heat transport changes are primarily due to variations in the westward flow of relatively warm water across the northern end of the section. Weak (strong) westward flow and large (small) eastward heat flux coincides with equatorward (poleward) displacements of the latitude of zero wind stress curl.

1. Introduction

The Antarctic Circumpolar Current (ACC) provides the primary means by which mass, heat, salt, and other properties are transferred between the ocean basins. The interbasin connection provided by the ACC is therefore a key element in the global overturning circulation. The vigorous interbasin exchange accomplished by the ACC also opens the possibility of oceanic teleconnections, where anomalies formed in one basin may be carried around the globe to influence climate at remote locations [e.g., *White and Peterson*, 1996; *White and Cherry*, 1998].

For these reasons the transport of the ACC has been a subject of intense oceanographic interest for decades. While calculation of the geostrophic transport relative to a deep reference level from measurements of density was straightforward, the barotropic flow presented a more serious challenge. Early attempts to measure the barotropic flow using short-term current meter records led to wildly different transport estimates (see *Peterson* [1988] for a review). The discrepancy between these early direct velocity measurements inspired a concerted effort during the International Southern Ocean Studies (ISOS) experiment in Drake Passage. High-resolution hydrographic sections revealed the banded nature of the ACC and explained the earlier current meter results: an instrument deployed in one of the strong narrow fronts would give vastly different results from one deployed in the weak flow between the jets. During ISOS, current meter moorings and pressure gauges were deployed across the passage and maintained for a number of years. The result of this dedicated effort was an estimate of the mean absolute transport of the ACC: 134±13 Sv [*Whitworth*, 1983; *Whitworth and Peterson*, 1985]. This number is often taken, along with the transport of the Gulf Stream through the Florida Straits, as one of the few "knowns" in the oceanographer's canon.

The ISOS measurements also revealed the variability of the ACC. Deep pressure gauges moored on either side of the passage provided a 4 year record of the pressure

Copyright 2001 by the American Geophysical Union.

Paper number 2000JC900107
0148-0227/01/2000JC900107$09.00

Table 1. Occupations of the WOCE SR3 Repeat Hydrographic Line

Cruise	Date	Number of Stations	Reference
AU9101	October 1991	24	*Rintoul and Bullister* [1999]
AU9309	March 1993	47	*Rosenberg et al.* [1995a]
AU9407	January 1994	53	*Rosenberg et al.* [1995b]
AU9404	January 1995	51	*Rosenberg et al.* [1996]
AU9501	July 1995	54	*Rosenberg et al.* [1997]
AU9601	September 1996	57	*Rosenberg et al.* [1997]

difference across the passage, which could be related directly to changes in net transport through the passage [*Whitworth and Peterson*, 1985]. The pressure records showed that the transport varied by about 15–20 Sv on timescales of a few days [*Whitworth*, 1983]. Transport moorings (consisting of temperature and/or conductivity sensors at 6-7 levels moored on the 2500 m isobath) on either side of the passage provided a 1 year record of baroclinic transport variability. While the overall consistency in hydrographic structure revealed on dif-

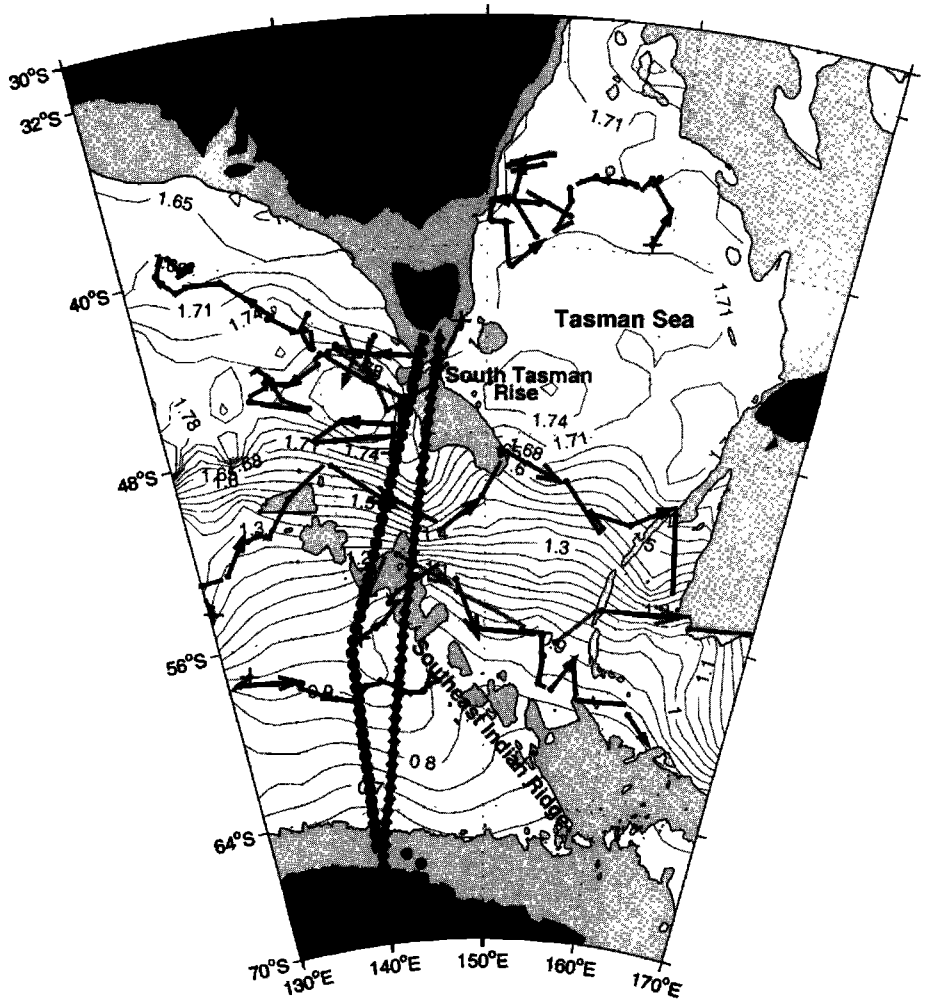

Figure 1. Location of the WOCE SR3 section (dots) and the SURVOSTRAL high density XBT line (diamonds). Contours are dynamic height at 500 m relative to 3000 m from the station data set (not the mapped fields) of *Gouretski and Jancke* [1998]; the field is mapped using a biharmonic method [*Sokolov and Rintoul*, 1999]. Depths less than 3000 m are shaded. Trajectories of several Autonomous Lagrangian Circulation Explorer (ALACE) floats [*Davis et al.*, 1992] are shown. The floats are deployed at approximately 950 dbar. The deployment location is indicated with a +. The length of each segment represents the drift over 27 days.

ferent transects across Drake Passage [e.g., *Reid and Nowlin Jr.*, 1971] has contributed to an emphasis on the barotropic component of the variability, the baroclinic variability from the dynamic height moorings is of comparable magnitude to the absolute transport variability inferred from the pressure gauges, although the former varies on longer timescales.

Most of what we know about the mean flow and variability of the ACC is based on these ISOS results in Drake Passage. No similar measurement program had been carried out at other longitudes until the World Ocean Circulation Experiment (WOCE). During WOCE the transport of the ACC was monitored at the Southern ocean "chokepoints," using repeat conductivity-temperature-depth (CTD) and expendable bathythermograph (XBT) sections, pressure gauges, moored instruments, and remote sensing. In this paper we present results from six occupations of the WOCE repeat hydrographic section (SR3) across the Australian chokepoint section. (The use of the term chokepoint, while common, is perhaps misleading for sections as long as those south of Africa (≈4000 km) and Australia (≈2500 km).)

We describe the primary circulation features between Tasmania and Antarctica and quantify their baroclinic transport variability. Variability in the net fluxes of mass, heat, salt, and nutrients is documented and related to changes in specific current branches south of Australia. In particular, the interbasin exchange of properties south of Australia is shown to be sensitive to variations in the strength of westward flow observed across the northern end of SR3. These changes are shown to be linked to meridional shifts in the latitude of zero wind stress curl. The results are compared to earlier measurements from Drake Passage. Finally, we discuss the implications of the observed transport variability for interbasin exchange and for the representativeness of single occupations of hydrographic lines, as obtained during the WOCE "one-time" survey.

2. Data

The WOCE SR3 section was occupied six times during the 5 years between October 1991 and September 1996, covering each season of the year (Table 1). In each case, CTD stations were occupied to within 10-15 m of the seafloor with a nominal station spacing of 56 km, with tighter station spacing in regions of steep dynamic or bottom topography. The first occupation in October 1991 had coarser spatial resolution in some locations because of extreme weather and sea ice conditions. In addition, the sections do not exactly coincide at the southern end, where the ship was often required to divert from the nominal cruise track to find a way through the sea ice. Details concerning the CTD calibration, bottle analyses, problems encountered, and sampling carried out on each cruise can be found in a series of technical reports [*Rosenberg et al.*, 1995a, 1995b, 1996, 1997]. In the following, all density values quoted are neutral density γ_n [*Jackett and McDougall*, 1997] in units of kg m^{-3}, all salinity values are on the practical salinity scale, and all temperatures are potential referenced to the sea surface. The emphasis of this paper is on the baroclinic transport variability. Readers interested in a more complete discussion of the water masses and circulation at SR3 are referred to *Rintoul and Bullister* [1999]. *Yaremchuk et al.* [this issue] provide a different perspective on the mean flow and variability at SR3, based on results of a variational model.

Figure 1 shows the location of the SR3 section, the mean dynamic topography at 500 m relative to 3000 m and the bathymetry in the area. The strongest flow of the ACC is found on the north side of the Southeast Indian Ridge. Near 140°E the ridge and the current turn to the southeast. The South Tasman Rise lies north of the ACC and reaches sufficiently close to the sea surface (<1500 m depth) to provide a significant obstacle to flow in this region. Streamlines associated with the eastward flow south of the ridge and west of 140°E turn to the north upon encountering the shoaling topography of the ridge and then turn back to the southeast again once they cross the ridge.

3. Results

3.1. Mean Density Structure

To provide a context for the transport discussion to follow, Figure 2 shows a section of neutral density along SR3 constructed from a mean of the six repeat sections. Density surfaces generally slope upward to the south across the section. At the northern end of the section the overall trend of the neutral surfaces is reversed, and density surfaces shoal to the north to form a shallow isopycnal bowl between 50°S and 44°S. A thick pycnostad with density between 26.9 and 27.0 fills the upper part (150-600 m) of the bowl. This is the local variety of Subantarctic Mode Water (SAMW) formed by deep convection in winter.

The horizontal density gradients extend from the sea surface to the seafloor. Assuming a deep reference level (the choice of reference level is considered in more detail below), the mean baroclinic structure illustrated in Figure 2 suggests the following circulation: westward flow north of 46°S, a broad band of strong eastward flow between 50° and 54°S, weak flow between 54° and 58°S, and a broad band of moderate eastward flow between 58° and 66°S.

The mean field of course smooths some features of the flow revealed in the individual sections. To illustrate the variability of the baroclinic structure in a compact way, dynamic height at the sea surface relative to 2000 m is shown for each of the sections (Figure 3). The greatest variability is found at the northern end of the section. For example, the relatively shallow isopycnal bowl between 50° and 44°S in the mean field is the result of averaging sections with deep bowls (October 1991 and January 1995) with sections with flatter isopycnals (January 1994, July 1995, and September 1996). The southward decrease in dynamic height between 50° and 54°S is relatively steep in September 1996 and Jan-

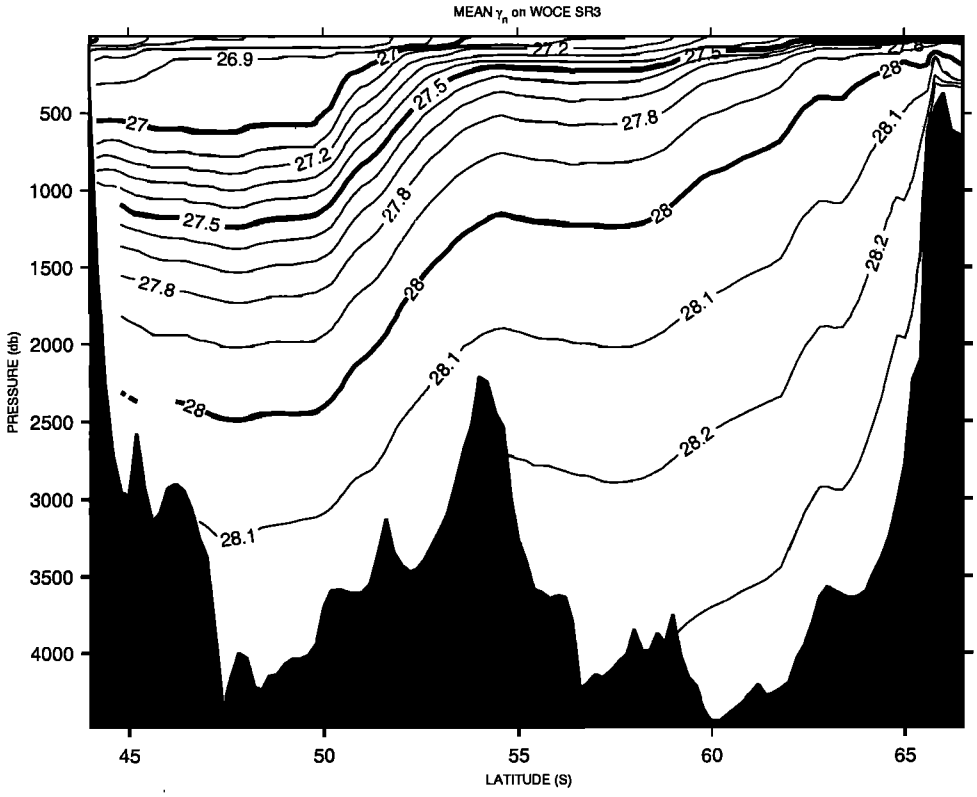

Figure 2. Mean section of neutral density anomaly (kg m^{-3}) from six occupations of SR3.

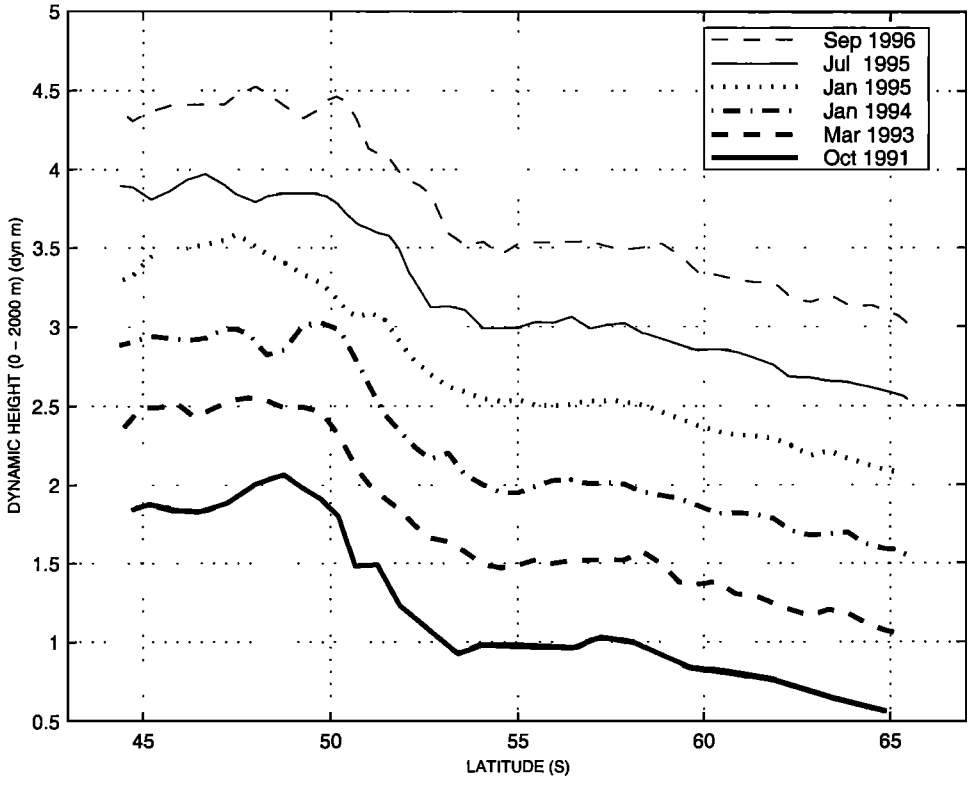

Figure 3. Dynamic height (dyn m) at the sea surface relative to 2000 m on six occupations of SR3. Each curve is offset by 0.5 dyn m.

uary 1994 and more gradual in July 1995. Two sections (January 1994 and September 1996) show a dip in dynamic height north of the ACC, indicating the presence of a cyclonic meander or eddy pinched off from the Subantarctic Front (SAF).

3.2. Choice of Reference Level

A deep reference level is usually assumed for the ACC, based primarily on evidence from direct velocity measurements in Drake Passage. Current meter records there show that the ACC reaches to great depth and, more quantitatively, that referencing geostrophic calculations to velocity measurements across the passage gives similar transports to estimates made assuming a level of no motion at the deepest common depth at each station pair [*Whitworth et al.*, 1982; *Whitworth*, 1983].

Rintoul and Bullister [1999] show that a near-bottom reference level is consistent with water mass properties and float trajectories at SR3 (samples of the latter are shown in Figure 1), except at the southern end of the section. There they argue that Adelie Land Bottom Water [*Rintoul*, 1998] and Ross Sea Bottom Water formed to the east of SR3 must flow west on average, requiring a reference level between newly formed Antarctic Bottom Water (AABW) and older Circumpolar Deep Water (CDW) above. They took a reference level coincident with the $\theta = -0.2°C$ isotherm, which in this region also approximately coincides with the 34.682 isohaline and the γ_n=28.318 surface. We adopt the same strategy here.

Westward flow over the upper continental slope, associated with the Antarctic Slope Front (ASF) [*Jacobs*, 1991; *Whitworth et al.*, 1998], is found at many locations around the continent, including at SR3. Current meter measurements in the eastern Weddell Sea indicate strong westward bottom velocities associated with this flow [*Fahrbach et al.*, 1994]. Upper ocean velocities inferred from ice drift [*Tchernia and Jeannin*, 1983; *Heil and Allison*, 1999], surface drifters, and acoustic Doppler current profiler measurements [*Bindoff et al.*, 2000] are westward across the southern end of the SR3 section. For those sections that extended as far as the continental shelf a reference level was chosen to give westward flow at all depths in the ASF.

The velocity at the deepest common depth is held constant through the "bottom triangle" beneath the deepest common depth at each station pair. Because the reference level is close to the bottom, the transport estimates are insensitive to the treatment of the bottom triangles.

While the water properties and ALACE trajectories provide some guidance on a reasonable choice of reference level, the reader should keep in mind that all the results shown are for the baroclinic transport alone. (Throughout the paper, baroclinic is used to refer to velocity and transport relative to a reference level; barotropic is used to refer to the velocity at the reference level). Direct velocity measurements in other parts of the Southern Ocean suggest that significant barotropic flows exist. The geostrophic transport rela-

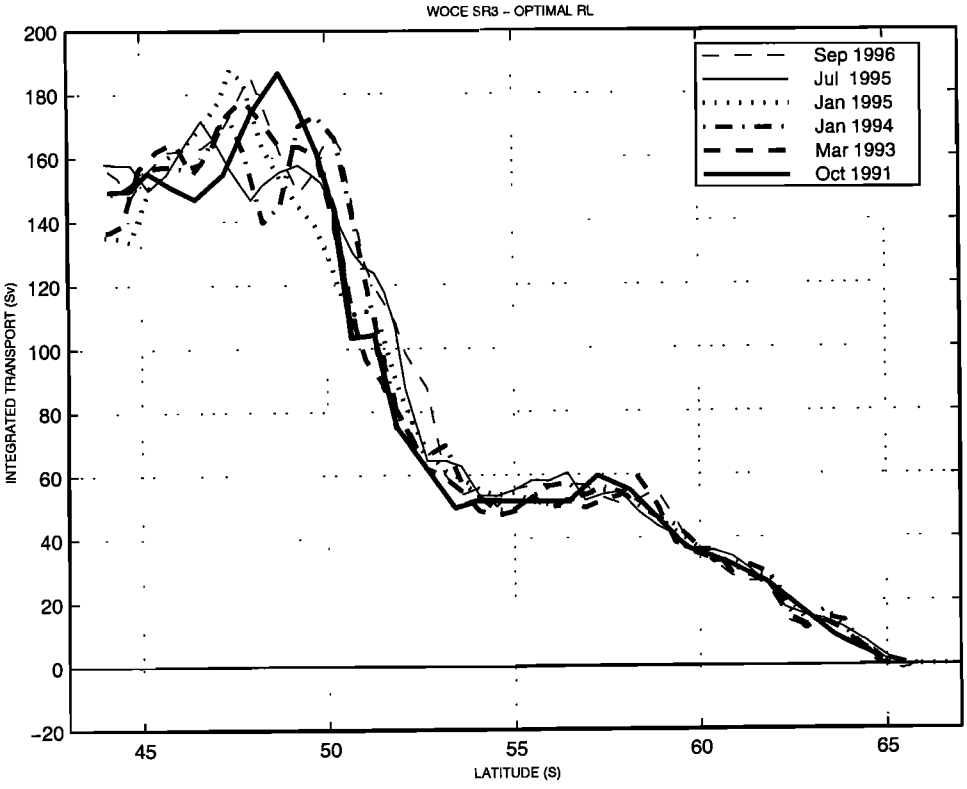

Figure 4. Cumulative volume transport (Sv) integrated from south to north across six occupations of SR3 relative to a best guess reference level (see text).

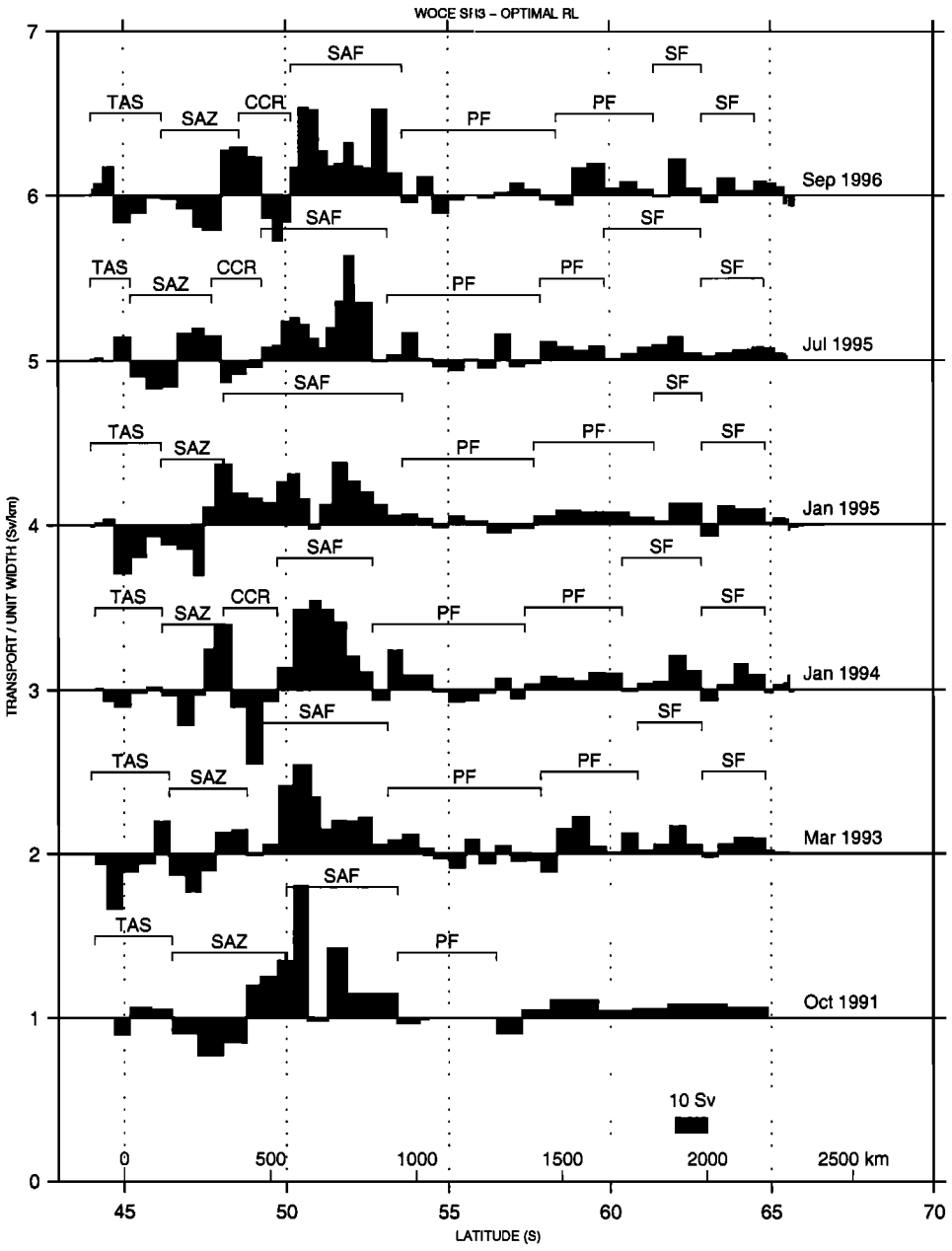

Figure 5. Transport per unit width for six occupations of SR3. Area under each curve is proportional to transport; the scale bar equals 10 Sv. Eastward flow is positive. Curves are offset by 1 Sv km^{-1}. The location of major fronts and circulation features are shown above each plot: TAS, Tasman outflow; SAZ, Subantarctic Zone recirculation; CCR, cold core ring or meander; SAF, Subantarctic Front; PF, Polar Front; SF, southern ACC front. The brackets indicate the limits used to sum up the transports of individual current branches.

tive to any choice of reference level may not give a good indication of the absolute transport.

3.3. Vertically Integrated Baroclinic Transport

The distribution of vertically integrated transport with latitude is illustrated in Figures 4 and 5. (The reader may also find it useful to refer to the schematic summary of the circulation in Figure 6, which is discussed in section 3.7.) The net baroclinic transport (relative to the "best guess" reference level described above) has a mean of 147 Sv and a range of 135–158 Sv (Figure 4). (Transports relative to other reference level choices are discussed in section 4). The 1991 section does not extend as far south as the later sections; the origin for the cumulative transport curve for this section is taken to be the mean of the other five sections at the latitude of the southernmost station pair in 1991.

The net transport south of 55°S is 50 Sv to the east (Figure 4). Three weak transport maxima occur within this broad band of eastward flow (Figure 5). The trans-

port peak between 58° and 60°S corresponds to the southern branch of the Polar Front (PF) [*Rintoul and Bullister*, 1999], a feature defined by a deepening of the temperature minimum layer to the north (and at some longitudes by a sea surface temperature (SST) gradient, hence sometimes called the "surface expression" of the PF). The maxima near 62° and 64°S coincide with fronts whose characteristics are similar to the "southern ACC front" (SACCF) of *Orsi et al.* [1995]. At SR3 the SACCF appears to split into two branches or to meander across the section, perhaps in response to the topographic bump seen near 63°S in Figure 2. The "southern boundary" of the ACC (SB) [*Orsi et al.*, 1995] sometimes merges with the SACCF (e.g., July 1995, Figure 5) and sometimes appears as a distinct weak core of eastward flow (e.g., January 1995). The latitude and transport of the fronts south of 55°S are remarkably similar on each of the six sections.

The cumulative transport increases by about 100–120 Sv between 55° and 48°S (Figure 4). The rapid increase in transport reflects the contribution of the SAF and the northern branch of the PF. Each section shows a number of transport maxima that correspond to multiple cores of the SAF and the northern PF (Figure 5). The picture of the ACC as consisting of a few well-defined fronts separated by regions of uniform water mass properties, developed from Drake Passage experience [e.g., *Nowlin and Clifford*, 1982], does not apply to the ACC at SR3.

Each of the curves in Figure 4 slopes down to the north at the northern end of SR3, corresponding to westward flow. The strength of the westward flow varies between sections: in January 1995 the net transport between the cumulative transport maximum at 48°S and the Tasmania coast is 50 Sv to the west; in July 1995 the corresponding number is about 10 Sv (Figure 4). In particular, the cumulative transport curves for two cruises (March 1993 and January 1995) diverge from the other four north of this latitude. Flow across both sections is strongly westward north of 46°S, between the South Tasman Rise and the Tasmanian continental slope (Figure 5). As a result, the net baroclinic transport across the section at these times is about 20 Sv lower than the other sections.

3.4. Origin of Westward Flow South of Tasmania

Rintoul and Bullister [1999] identify two cores of westward flow across the October 1991 section: westward flow associated with an anticyclonic recirculation in the Subantarctic Zone (SAZ) and an outflow of water from the Tasman Sea. The source of the westward flow across SR3 can be most clearly illustrated by comparing θ–S curves at the depth of the salinity minimum of the Antarctic Intermediate Water (AAIW). For example, Plate 1 shows θ–S curves from the northern end of the January 1995 section. Stations south of 46°S fall in a family of curves with typical salinity minimum water properties of about θ=4°C, S=34.35. Stations in the eastward flow between 48° and 50°S (blue curves) have similar θ–S characteristics to stations in the westward limb of the recirculation between 46° and 48°S (red curves). These profiles therefore suggest that a pool of AAIW recirculates north of the ACC.

Stations north of 46°S on the same occupation of SR3 are distinctly warmer and saltier (green curves in Plate 1) than stations to the south. Typical values characterizing the salinity minimum water are θ=4.5°–5.0°C and S=34.44. Geostrophic calculations suggest this water is also flowing to the west. The water mass properties are consistent with this interpretation: the θ–S curves north of 46°S on SR3 overlap the envelope of θ–S curves observed at 43°S in the southern Tasman Sea (magenta curves in Plate 1), suggesting the warm salty variety of AAIW is carried from the Tasman Sea and flows south and west across SR3. Property distributions below the AAIW suggest the Tasman outflow extends to the seafloor [*Rintoul and Bullister*, 1999].

The envelope of θ–S curves at 43°S in the Tasman Sea is broad. The AAIW there is a mixture of cold, fresh, high oxygen AAIW entering the Tasman Sea from the south, and warm, salty, low-oxygen AAIW entering the Tasman Sea from the east, north of New Zealand [*Wyrtki*, 1962; *Sokolov and Rintoul*, 2000]. The properties of the AAIW entering the basin from the east are illustrated by θ–S curves from the East Australia Current at 30°S (black curves in Plate 1).

The dynamic topography map in Figure 1 illustrates the connection between the flow at SR3 and the regional circulation. The 1.71 dyn m contour loops through the southern Tasman Sea before turning back to the west, consistent with weak outflow from the Tasman Sea. This pattern agrees with observations at 155°E (WOCE P11S), which show sharp property fronts near 38°S, indicating that AAIW entering from the south reaches no farther north before turning back to the south [*Sokolov and Rintoul*, 2000]. More confined anticyclonic recirculations are evident immediately north of the ACC to the east and west of the South Tasman Rise. Part of the recirculation to the west of the South Tasman Rise, which is partially crossed by SR3, continues westward across the Great Australian Bight.

Both branches of westward flow also appear in float trajectories (Figure 1) [see also *Davis*, 1998]. Two floats deployed in the southwest Tasman Sea moved south and westward through the gap between Tasmania and the South Tasman Rise; a third float deployed in the gap also moved westward. No floats moved eastward through this gap. The Tasman Sea floats also support the notion that the southern Tasman Sea is generally characterized by sluggish and variable flow, with little net inflow from the south extending beyond about 38°S. Three floats deployed along SR3 west of the South Tasman Rise carried out an anticyclonic loop between about 139° and 146°E, 49° and 45°S, consistent with the idea that the SAZ recirculation on SR3 is at least in part a local feature, as inferred from the water mass properties. The large spatial scale and relatively long transit times of the anticyclonic loops (typically more than 150 days to complete a circuit) suggest the floats

are tracing a permanent but variable part of the general circulation, rather than a transient eddy. While the number of float trajectories in the region is small, and inadequte to provide a quantitative reference velocity for transport calculations, all of the trajectories are consistent with the sense of flow inferred from water mass properties and a deep reference level.

The westward flows across the northern end of SR3 vary with time (Figure 5). The January 1995 section illustrated in Plate 1 is an example of a time when both the SAZ recirculation and the Tasman outflow are well developed. In contrast, in January 1994 and July 1995 there was little Tasman Sea water present, and the flow north of 46°S was weakly westward (January 1994) or eastward (July 1995). The transport of the SAZ recirculation varies from a maximum of 35 Sv in October 1991 to a minimum of 12 Sv in March 1993.

3.5. Transport in Density Layers

Another important aspect of the variability at SR3 is the change in transport of individual water masses. Are periods of relatively high baroclinic transport associated with a top-to-bottom increase in the ACC affecting all layers, or is an increase in net transport associated with larger transports of particular layers?

Plate 2 shows the transport across each SR3 section in neutral density layers. The net transport of intermediate, deep, and bottom water is very steady: transport of the AAIW and deeper layers varies about the mean for each layer by $< \pm 2$ Sv. Nevertheless, the two low-transport sections (March 1993 and January 1995, red and magenta curves in Plate 2), are systematically lower in transport in all density layers from 26.9 to 28.3, while the converse is true for the high-transport July 1995 and September 1996 sections.

The greatest transport variability occurs in layers lighter than $\gamma_n = 27.0$. In particular, transport of SAMW ($\gamma_n = 26.9$–27.0) varies from 4 to 15.5 Sv. Part of this variability is seasonal: in winter, there is little water on SR3 lighter than 26.8; in summer, warming converts SAMW to lighter densities. Therefore we expect larger transports in the 26.8–26.9 density class in winter, and larger transports in lighter layers in summer, as seen in Plate 2.

The seasonal conversion of water from one density class to another, however, is not the whole story. The net transport across each section summed over density layers lighter than 27.0 shows the same pattern as noted above for deeper layers: sections with low total transport have less water flowing east in the light layers, while sections with high total transport have larger transport in light layers: the mean of the two low-transport sections (March 1993 and January 1995) is 9.0 Sv; the mean of the two high-transport sections is 17.4 Sv.

3.6. Temperature, Salt, and Nutrient Transports

The westward flow south of Tasmania is negatively correlated with net eastward transport across SR3: the sections with strong westward flow at the northern end of the section (March 1993 and January 1995, Figure 5) also have low net eastward transport (Figure 4). The impact of strong westward flow on the net transport of properties other than volume can be even more dramatic for properties whose concentration varies with latitude.

The net transport of temperature, salt, nutrients and oxygen is included in Table 2. The range of temperature flux is 139°C Sv, or 0.57 PW_{0C} (where we use PW_{0C} to represent the conversion of temperature flux to units of heat flux relative to 0°C obtained by multiplying the temperature flux by the density and specific heat; because this is not strictly a heat flux when there is a nonzero mass flux (e.g., a change of temperature units to K would give a different number), we use the subscript to indicate the temperature reference used). Changes in baroclinic heat transport may not indicate changes in the absolute heat transport between the basins if the barotropic flow can carry enough heat to compensate the baroclinic variations. Such compensation would require that the barotropic heat transport vary on a similar timescale, with similar magnitude but opposite sign, to the observed baroclinic variations. While the mechanism that would link the barotropic and baroclinic variability in this way is not obvious to us, we cannot rule out the possibility in the absence of measurements of the barotropic flow.

Nutrient and oxygen fluxes across a single section are difficult to interpret in isolation, and there are few estimates with which to compare our results. While nutrient fluxes are not often quoted in papers such as this, the nutrient fluxes are straightforward to compute and the nutrient budgets provide valuable constraints on the

Table 2. Baroclinic Property Fluxes Across SR3

Cruise	Volume, Sv	Temperature, °C	Heat, PW_{0C}	Salt, kmol s^{-1}	Nitrate, kmol s^{-1}	Phosphate, kmol s^{-1}	Silicate, kmol s^{-1}	Oxygen kmol s^{-1}
AU9101	149	419	1.87	5144	4512	332	8931	33786
AU9309	137	369	1.65	4705	4285	286	8091	29879
AU9407	149	431	1.93	5132	4448	309	8363	33918
AU9404	135	338	1.51	4653	4195	290	8103	30710
AU9501	158	477	2.13	5457	4596	322	8414	34851
AU9601	156	472	2.11	5379	4654	307	8714	34663

circulation [e.g., *Robbins and Toole*, 1997]. The use of such constraints requires knowledge of the variability of the fluxes. Table 2 shows the changes in the baroclinic transports of nitrate, phosphate, and silica are large relative to the meridional fluxes entering the subtropical gyres (which are usually assumed to be close to zero, given that there is no atmospheric pathway for nutrients and storage in the sediments at low latitudes is believed to be small). More study is required to understand the implications of the nutrient flux variability, and we encourage other authors to publish nutrient flux estimates. One possibility is that variations in the barotropic transport might compensate all or part of the baroclinic transport variability, as noted above for temperature. However, given that the vertically averaged temperature tends to increase toward the north while the vertically averaged nutrient concentrations tend to decrease to the north, it might be difficult for the barotropic flow to simultaneously compensate the baroclinic variability in both temperature and nutrient fluxes. For example, a barotropic flow to the east across the southern half of the section and to the west across the northern half would decrease the eastward temperature flux while increasing the eastward nutrient fluxes.

3.7. Transport Summary

Figure 6 summarizes the mean baroclinic transport and its variability south of Australia. Six major current branches are identified, although the boundary between each current branch or front is somewhat arbitrary. Traditional definitions of ACC fronts (e.g., the northernmost extent of a particular isotherm) generally coincide with a single station pair at the core of the front, while the shear and transport associated with the front may span several station pairs. Because the focus here is on transport, we have relied on extrema and

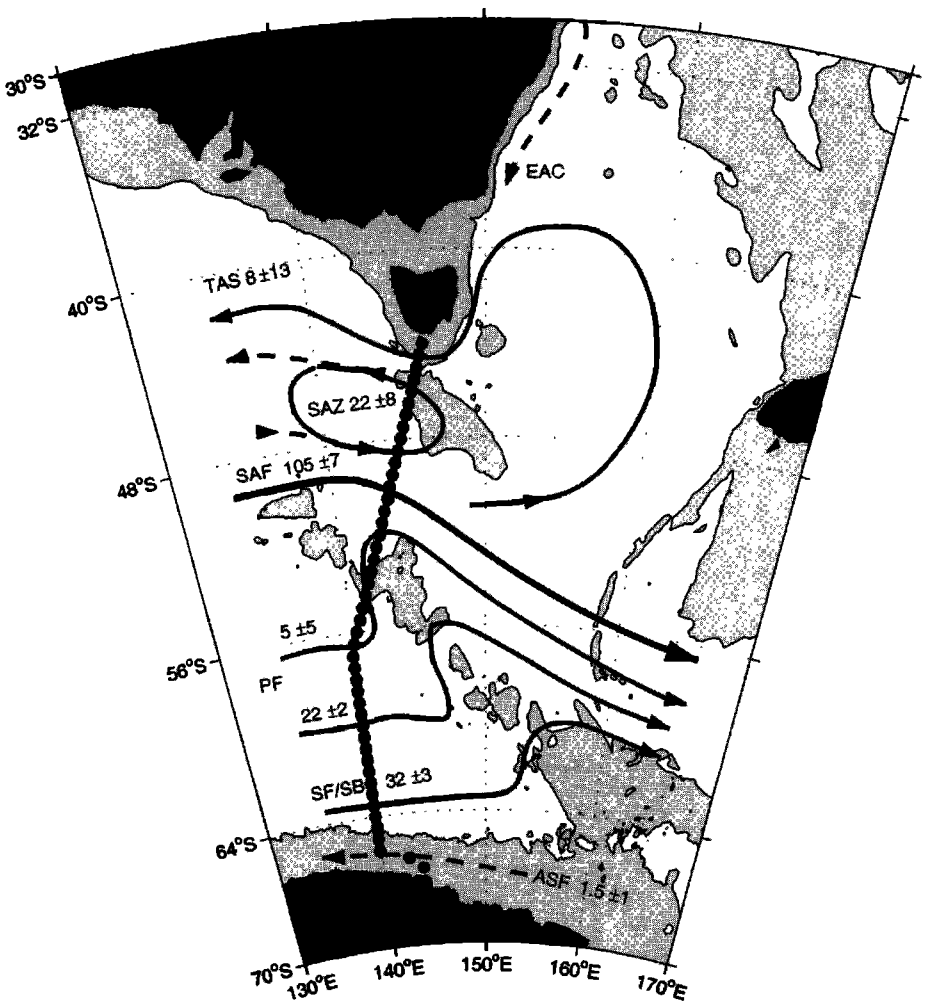

Figure 6. Schematic summary of main circulation features on SR3: EAC, extension of East Australian Current; TAS, Tasman outflow; SAZ, Subantarctic Zone recirculation; SAF, Subantarctic Front; PF, Polar Front; SF, southern ACC front; SB, southern boundary of the ACC; ASF, Antarctic Slope Front. Numbers give top-to-bottom transports in Sv (mean ±1 standard deviation). See text and Figure 5 for a description of the integration limits for each current branch or front.

zero crossings in the transport versus latitude curve for each section, as well as water properties, to define the limits of each front (see Figure 5). By using a phenomenonological definition (rather than, for example, a band of latitudes) to define the fronts we avoid introducing transport variability caused by shifts in latitude or orientation of the fronts. The transports in Figure 6 are integrated over the entire water column; the uncertainties associated with each branch are ±1 standard deviation. The schematic streamlines are drawn to be consistent with climatological dynamic height (Figure 1), float trajectories [*Davis*, 1998], and additional hydrographic and XBT data from the region, as described below.

Water originating in the Tasman Sea can be clearly identified by its water properties, as described in section 3.4. Summing the transport over station pairs with Tasman Sea water results in a westward flow of 8±13 Sv. As shown in Figures 1 and 6, part of the northward inflow to the Tasman Sea returns to the south over the Tasmanian continental slope and continues west across SR3. The large standard deviation indicates the variable nature of this flow. (Note that not all the SAMW and AAIW crossing SR3 turns north into the Tasman Sea; some continues to the east and enters the Pacific south of New Zealand.)

To quantify the transport and variability of the recirculation identified in the SAZ, we define its northern edge to be the southern limit of Tasman Sea-influenced water and then integrate south to the point where the sense of flow reverses (i.e., the bottom of the isopycnal bowl north of the SAF). This gives the westward flow on the northern limb of the recirculation. An equal amount of the eastward flow south of this point is attributed to the recirculation; the remainder is taken to be part of the SAF, as described below.

The recirculation reaches from top-to-bottom, involves a substantial transport, and is somewhat variable in time (22±8 Sv). The zonal extent of the recirculation is not well defined by the hydrographic data. Since it is deep reaching, it is likely to be confined to the east by the relatively shallow South Tasman Rise. Hydrographic sections to the east and west of SR3 (e.g., 132°E [*Schodlock et al.*, 1997] and 155°E (WOCE section P11A) [*Rosenberg et al.*, 1995a]) do not show the deep isopycnal bowl north of the SAF that is so prominent on SR3, in agreement with Figure 1 which shows a tight recirculation confined between 135°E and the South Tasman Rise, embedded within a weaker anticyclonic circulation that extends across the Great Australian Bight.

The SAF is defined operationally to extend from the southern limit of the recirculation to the transport minimum between the SAF and the PF (where the location of the PF is defined in the traditional way as the northernmost extent of temperature minimum water cooler than 2°C near 200 m depth [*Botnikov*, 1963]). The mean transport of the SAF is 105 Sv and is surprisingly stable with time (standard deviation of 7 Sv). The dynamic height map in Figure 1 shows the SAF turns to the southeast after crossing SR3, staying roughly parallel to the Southeast Indian Ridge. Float trajectories are consistent with this shift to the south, and individual floats cross the Macquarie Ridge through one of three gaps, at 52°, 54°, or 56°S.

The northern branch of the PF is found between 53° and 54°S on all six occupations of SR3. It carries 5±5 Sv to the east. West of SR3, this front lies farther south (between 55° and 58°S [see, e.g., *Gordon and Molinelli*, 1982, Plate 141]); as the flow encounters the shoaling topography of the Southeast Indian Ridge, the front shifts equatorward, as might be expected for weak, deep reaching flow conserving potential vorticity.

Between 53° and 58°S, the flow across SR3 is weak and variable and the isopleths of all properties are relatively flat. This is consistent with flow nearly aligned with the section through this latitude band, as expected from climatological dynamic height (Figure 1), trajectories, and as indicated by the 5° of latitude northward deflection of isotherms in this latitude band on the SURVOSTRAL XBT section relative to their location on SR3 [*Rintoul et al.*, 1997].

These data sources suggest the southern PF also deflects to the north when encountering the ridge. Because the ridge is further east at these latitudes, the southern branch of the PF is not deflected north until after crossing SR3. Both the location (59°S) and the transport (24±3 Sv) of the southern PF are remarkably steady at SR3.

South of 60°S, the transport of the southern ACC front at 62°S and 64°S is also remarkably steady: 18 ±3 Sv and 11 ±3 Sv, respectively. The southern boundary of the ACC (SB) and the Antarctic Slope Front (ASF) are not very well resolved by the SR3 repeats. (The sea ice over the continental slope at this longitude is often deformed and mobile, making CTD operations difficult, even in summer.) This may contribute to the relatively high variability of the transport estimates there. The transport of the SB is 2.6±2.4 Sv, while the westward flow associated with the ASF is 1.4±0.9 Sv.

4. Discussion

The results summarized above concern only the baroclinic transport. Substantial barotropic flows likely occur in the Southern Ocean. For example, shipboard and lowered acoustic Doppler current profiler (ADCP) measurements have shown that significant barotropic velocities exist in some ACC fronts [*Heywood et al.*, 1999; K. A. Donohue et al., Absolute geostrophic velocity within the Subantarctic Front in the Pacific Ocean, submitted to *Journal of Geophysical Research*, 2000; hereinafter referred to as K. A. Donohue, submitted manuscript, 2000]. However, ADCP data is not yet sufficiently accurate to provide a reference for transport calculations across long sections [K. A. Donohue et al., submitted manuscript, 2000]. Quantitative direct estimates of the barotropic contribution would require sustained, spatially coherent, and highly accurate velocity measurements across the 2500 km span of the section, a very

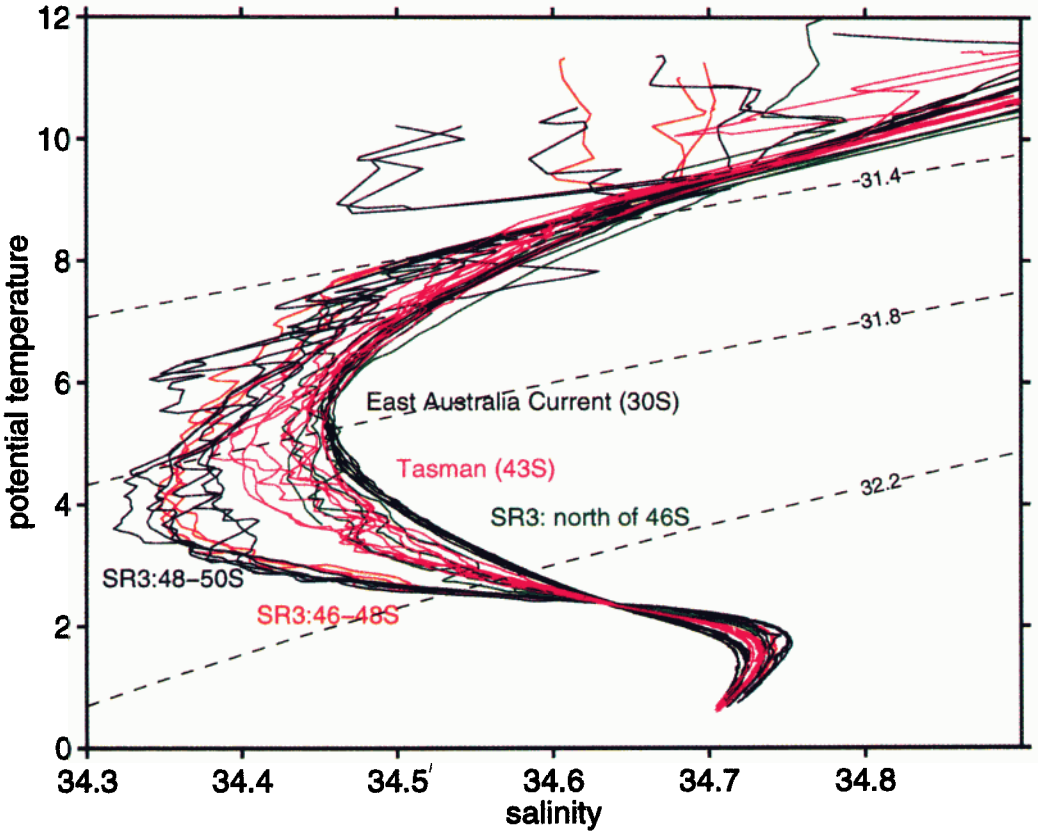

Plate 1. Potential temperature–salinity profiles from stations at the northern end of SR3 and from the Tasman Sea. (The Tasman Sea data at 43° and 30°S come from a 1989 R/V *Franklin* cruise FR8910; data are available from CSIRO Marine Research.) Dashed curves are density relative to 1000 dbar. The salinity minimum of the AAIW is warmer and saltier at the northern end of SR3 and similar in properties to AAIW in the southern Tasman Sea.

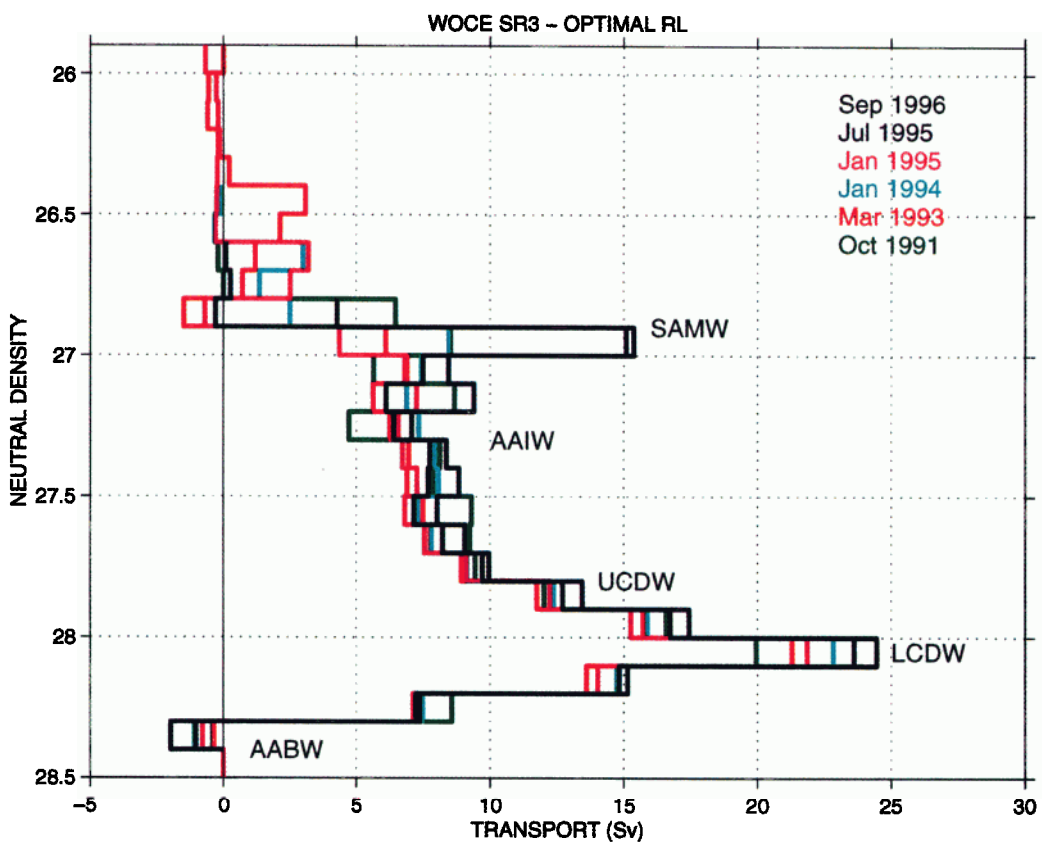

Plate 2. Variability of transport in neutral density layers for six occupations of SR3. SAMW, Subantarctic Mode Water; AAIW, Antarctic Intermediate Water; UCDW, Upper Circumpolar Deep Water; LCDW, Lower Circumpolar Deep Water; and AABW, Antarctic Bottom Water.

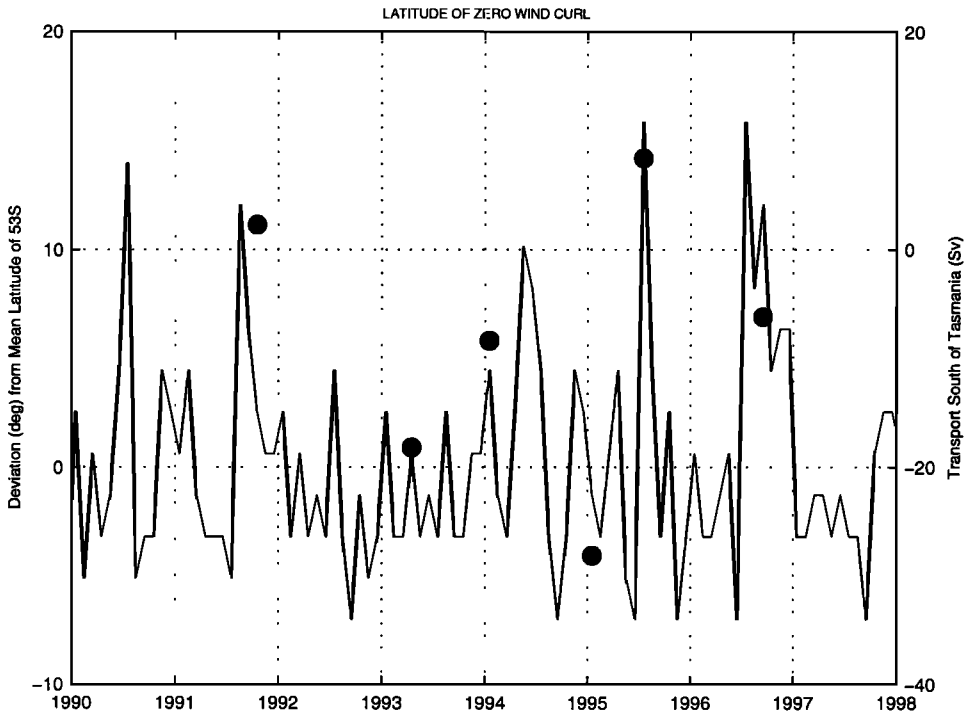

Figure 7. Deviation of the latitude of zero wind stress curl from its mean value of 53°S (solid line, in degrees of latitude). The curl of monthly wind stress values from the National Centers for Environmental Prediction (NCEP) reanalysis [*Kalnay et al.*, 1996] is averaged between 130° and 150°E and shown for the period 1980–1998. Solid dots indicate transport of Tasman Sea origin water across the northern end of SR3 for the six occupations of the section (in Sv, scale on right-hand side of plot). Positive values are toward the east.

challenging task (e.g., a 0.1 cm s^{-1} bias would carry 10 Sv across SR3). The results of three recent inverse calculations [*Yaremchuk et al.*, this issue; *Sloyan and Rintoul*, 2000a; *Ganachaud*, 1999] provide some evidence that the barotropic contribution to the net property fluxes across SR3 may be relatively small. The models differ substantially, but all agree that only small reference level velocities are needed to satisfy the model constraints, and their estimates of net property fluxes are similar to those found here.

4.1. Relationship Between Wind Stress Curl and Tasman Outflow

We have shown that the transport variability across SR3 is dominated by changes at the northern end of the section. The heat transport variability, in particular, reflects variations in the amount of warm water flowing west between Tasmania and the South Tasman Rise. A strong Tasman outflow can be thought of as a poleward shift of the subtropical regime. This view suggests looking for links between meridional shifts in wind stress curl and the strength of the Tasman outflow. In closed basins the zero of the wind stress curl marks the boundary between the cyclonic subpolar gyres and the anticyclonic subtropical gyres. While the zero curl line in the zonally unbounded Southern Ocean does not coincide with gyre boundaries in the same sense, it still marks the transition from subtropical (Ekman pumping) to subpolar (Ekman suction) regimes.

Figure 7 shows an eight year record of the latitude of zero wind stress curl south of Tasmania. The mean latitude is about 53°S. The median position is 2°–3°of latitude farther south, reflecting the fact that the zero curl line is most often near 55°S, with occasional large equatorward displacements that usually persist for a few months.

The solid dots in Figure 7 show the transport of the Tasman outflow across the six occupations of SR3. While the number of sections is small, a relationship appears to exist between meridional shifts of the zero curl line and westward transport; poleward shifts of the zero curl line (hence poleward shifts of the subtropical regime) correspond to large Tasman outflow. When the zero curl line shifts north to about the latitude of Tasmania (43°S), the transport is near zero or eastward. Figure 7 suggests that four of the six occupations of SR3 were made during periods when the zero curl line was anomalously far north. Hence our estimate of the mean transport of the Tasman outflow is likely biased low. On the basis of the mean position of the zero curl line the mean transport of the outflow is likely to be about 20 Sv. The strength of the Tasman outflow is correlated with the net eastward heat flux across the section, so our mean heat flux estimate may be biased high.

Figure 7 suggests meridional shifts in wind stress curl are likely to play an important role in regulating the variability in interbasin exchange south of Tasmania.

De Ruijter and Boudra [1985] used an eddy-resolving barotropic model to demonstrate a similar relationship between poleward shifts of the latitude of zero wind stress curl and enhanced interbasin exchange south of Africa. De Ruijter and Boudra speculated that variability in the inflow of warm Agulhas water to the Atlantic may have a significant impact on climate in that region; westward flow of relatively warm water south of Tasmania may influence southern Australian climate in a similar manner.

4.2. Comparison to Drake Passage

How do the baroclinic transport estimates south of Australia compare to Drake Passage, the only other location where repeat measurements have allowed the transport variability of the ACC to be assessed? *Nowlin and Clifford* [1982] calculated baroclinic tranport above and relative to 2500 m for five sections across Drake Passage occupied in 1975-1976 and found remarkably constant values: a mean of 87 Sv and a range of only ±1 Sv. *Whitworth* [1980] found slightly smaller values, with a wider range, and noted an apparent seasonal difference: the mean of 16 summer sections was 79±13 Sv and of 6 winter sections was 71±15 Sv. A 1 year record of transport above and relative to 2500 m from transport moorings on either side of the passage gave a mean value of 87 Sv, with a standard deviation of 5.5 Sv [*Whitworth*, 1983].

The transport above and relative to 2500 m south of Tasmania is substantially higher than that observed in Drake Passage. The mean of six CTD sections along SR3 is 107 Sv, with a range of 95–117 Sv (Table 3). A similar pattern is seen when transports relative to alternative reference levels between 2000 m and the bottom are compared: the baroclinic transport south of Tasmania is substantially higher in each case. At SR3 the baroclinic transport variations above 2500 m are not compensated by variations of opposite sign at greater depth. The transport above and relative to 2500 m is a nearly constant fraction (66±1.4%) of the transport relative to the bottom for each of the six SR3 sections. The transport variations result from shifts in the density field that affect the entire water column, near one or both endpoints of the section.

Another perspective on the difference in baroclinic structure between Drake Passage and SR3 can be gained by comparing dynamic heights at either side of the passages. Transport moorings deployed for 1 year in Drake Passage gave mean values of 1.37±0.05 and 0.58±0.02 dyn m at the northern and southern sides (for the dynamic height anomaly at 500 m relative to 2500 m) [*Whitworth*, 1983]. The corresponding mean values from six occupations of SR3 are 1.42±0.07 and 0.50±0.005 dyn m, respectively. That is, the dynamic height is both higher on the high (equatorward) side and lower on the low (poleward) side of the ACC at SR3. The much longer SR3 section extends 12° farther north and 3°farther south than Drake Passage and crosses lighter water north of the Subtropical Front and denser Antarctic water in the south. As found in Drake Passage, the variability of dynamic height anomalies at the northern end of SR3 is much higher than at the southern end.

The mean baroclinic transport across SR3 relative to the best guess reference level is 147±9.7 Sv. The variability is very similar to the standard deviation of absolute transport at Drake Passage (10.5 Sv) estimated by *Whitworth and Peterson* [1985]. The best estimate of the mean transport at Drake Passage is 134 Sv (125 Sv above 2500 m [*Whitworth and Peterson*, 1985] plus 9 Sv below 2500 m [*Whitworth*, 1983]), resulting in an apparent convergence of 13 Sv in the Pacific. To conserve mass in the Pacific basin as a whole, the difference in absolute transport between SR3 and Drake Passage must be balanced by outflow through the Indonesian passages and the Bering Straits (ignoring small mass transports due to evaporation, precipitation and runoff). Estimates of the transport of the Indonesian Throughflow range from -2 to 22 Sv, with a best guess of the mean likely to be about 10 Sv [*Cresswell et al.*, 1993; *Meyers et al.*, 1995]. About 1 Sv is believed to flow out of the Pacific through the Bering Straits [*Coachman and Aagaard*, 1988]. Given the uncertainty of the estimates (e.g., of the barotropic flow at SR3 and at the Indonesian throughflow and the uncertainty in the Drake Passage absolute transports), the close agreement is likely fortuitous.

The use of pressure gauges to monitor variability in absolute transport assumes that the variability is

Table 3. Baroclinic Volume Transports Across SR3 Relative to Different Reference Levels [a]

Cruise	Reference Level			
	2000 dbar, Sv	2500 dbar, Sv	DCD, Sv	BG, Sv
AU9101	87	107	160	149
AU9309	73	95	146	137
AU9407	87	109	165	149
AU9404	76	99	149	135
AU9501	91	115	169	158
AU9601	93	117	181	156

[a] DCD is the deepest common depth at each station pair and BG refers to the best guess reference level described in the text.

predominantly barotropic. However, measurements in Drake Passage indicate that the baroclinic variability, while smaller than the barotropic variability, is not negligible. During 1979, the baroclinic transport varied on longer time-scales, but the range (70–100 Sv) was comparable to that of the absolute transport (105 to 140 Sv) [*Whitworth*, 1983, Figure 7]. The absolute transport above 2500 m had a standard deviation of 8.5 Sv; the baroclinic transport above 2500 m had a standard deviation of 5.5 Sv [*Whitworth*, 1983]. Observations at SR3 suggest the baroclinic variability is of comparable magnitude to that at Drake Passage, so the assumption that the transport variability of the ACC is primarily barotropic may not be entirely valid.

4.3. Implications for Interbasin Exchange

Georgi and Toole [1982] (hereinafter referred to as GT82) used hydrographic sections spanning the ACC to estimate the exchange of heat and freshwater south of Africa, New Zealand and America. From the divergence they inferred the net air-sea exchange in individual basins. Their calculation was an early example of the power of direct ocean transport estimates to constrain estimates of air-sea exchange, but a number of factors contributed to introduce significant uncertainty in the inferred air-sea fluxes. Of most importance, GT82 ignored the Indonesian Throughflow on the basis of the *Wyrtki* [1961] estimate of 1-2 Sv of throughflow. More recent estimates suggest the throughflow is closer to 10 Sv in the mean and perhaps higher. Because the mean temperature of the throughflow ($\approx$ 24 °C [*Toole and Warren*, 1993]) is so high relative to that of the ACC, the existence of a significant throughflow has a major impact on the inferred net air-sea exchange in each basin. Second, in the absence of a section south of Australia, GT82 used a section south of New Zealand and assumed there was little net flow through the Tasman Sea. Third, in the absence of direct measurements of the barotropic flow, GT82 applied a uniform barotropic velocity at the African and New Zealand sections to make the volume transport there equal that at Drake Passage. Finally, only at Drake Passage were repeat sections available to determine a representative mean field.

In Table 4 we repeat the GT82 calculation including an estimate of the throughflow contribution and replacing the New Zealand section with the volume-transport-weighted temperature at SR3. Including the throughflow gives a very different impression of the interbasin flux and net air-sea heat exchange in the Indian and Pacific basins. Assuming a throughflow of 10 Sv with a transport-weighted temperature of 24°C and using the SR3 volume-transport-weighted temperature, the Indian basin is found to lose -0.4 PW of heat (rather than gain 0.6 PW in GT82) and the Pacific bain gains 0.7 PW of heat (rather than losing -0.3 PW).

Inverse models that use a variety of constraints to determine the distribution of the barotropic velocity (rather than assuming a constant value as in GT82) are probably a more effective way to determine the interbasin exchange of heat. As shown in Table 4, when the GT82 calculation is updated to account for the throughflow and a more representative section south of Australia, the results agree in sign with three recent global or hemispheric inverse models. The magnitudes are reasonably consistent with two of the inverse estimates [*Macdonald*, 1998; *Sloyan and Rintoul*, 2000b]. The model of *Ganachaud* [1999] has stronger heat gain in the Pacific and stronger heat loss in the Indian and Atlantic, as a result of a stronger Indonesian Throughflow and weaker eastward heat transports south of Africa and Australia.

The overall picture is of heat gain in the Pacific, which is exported to the other basins. This pattern might at first glance be taken as support for the picture of the global conveyor developed by *Gordon* [1986] and *Broecker* [1991], where North Atlantic Deep Water (NADW) upwells and is warmed in the Pacific and returns via the Indian Ocean as relatively warm inflow to the Atlantic. However, significant heat input in the Pacific is required even if the net inflow to the Pacific (required to balance the outflow via Indonesia) is made up of relatively warm upper layer water. For example, the warmest water with significant eastward transport across SR3 is SAMW, with a temperature of about 9°C. A heat input of 0.6 PW is required to convert 10 Sv of 9°C water to 24°C, the temperature of the Indonesian Throughflow (similar to the net heat flux into the Pacific estimated by the analyses summarized in Table 4). If the net inflow into the Pacific was made up of much cooler deep water, an even greater heat input would be required.

4.4. Representativeness of the WOCE One-Time Survey

Most of the WOCE global survey consisted of one-time occupations of hydrographic sections. The repeat sections like SR3 provide a means of assessing the possible alias or bias introduced by the availability of only single realizations of a complex, temporally evolving circulation.

Figure 6 shows that the transport of the ACC itself does not vary much with time; variability in the net transport south of Australia depends primarily on changes in the flow north of the ACC. Of most significance for the net transport of properties between the Indian and Pacific basins is the variability in the westward flow of relatively warm and salty water at the northern end of SR3. A strong Tasman outflow results in a low net eastward transport of heat and salt, as well as volume, across the section.

For example, the temperature flux varies over a range of 139°C Sv, or 0.57 PW_{0C}. These variations in heat flux are comparable to meridional heat fluxes at midlatitudes of the south Indian and Pacific basins. Changes in the baroclinic heat transport south of Australia may be compensated in a number of ways: changes in the heat storage, either local or basin-scale; changes in the zonal heat flux entering the Indian basin south of Africa or leaving the Pacific through Drake Passage; changes

Table 4. Interbasin Exchange of Volume and Temperature Between the Atlantic, Indian, and Pacific Basins[a]

Africa	Δ Indian, PW	Aus-Indo	Δ Pacific, PW	Drake	Δ Atlantic, PW	Africa
		Georgi and Toole [1982]				
127 Sv 240 °C Sv	+0.6	127 Sv 395 °C Sv	-0.3	127 Sv 320 °C Sv	-0.3	127 Sv 240 °C Sv
		Georgi and Toole [1982] + Indonesian Throughflow				
127 Sv 240 °C Sv	-0.2	137-10 Sv 426-240 °C Sv	+0.5	127 Sv 320 °C Sv	-0.3	127 Sv 240 °C Sv
		Georgi and Toole [1982] + Indonesian Throughflow + SR3				
127 Sv 240 °C Sv	-0.4	137-10 Sv [illegible]-240±28 °C Sv	+0.7	127 Sv 320 °C Sv	-0.3	127 Sv 240 °C Sv
		Macdonald [1998]				
144 Sv 278±96 °C Sv	-0.1	151-7 Sv 415-175 ±103 °C Sv	+0.4	144 Sv 343±65 °C Sv	-0.2	144 Sv 278±96 °C Sv
		Sloyan and Rintoul [2000a,b]				
135 Sv 300±24 °C Sv	-0.3	145-10 Sv 461-240±12°C Sv	+0.5	135 Sv 344±5 °C Sv	-0.2	135 Sv 300±24 °C Sv
		Ganachaud, [1999]				
139 Sv 183±56 °C Sv	-0.7	154 - 15 Sv 346 - 332 °C Sv	+1.2	140 Sv 317±34°C Sv	-0.5	139 Sv 183±56°C Sv

[a] Columns labeled Δ give the difference between the heat transport at the sections bounding each basin, or the net heat exchange in each basin; positive values indicate a heat gain by the ocean. "Aus-Indo" shows the transports across the Australian ACC chokepoint section minus the Indonesian Throughflow. The table compares values from the original *Georgi and Toole* [1982] calculation, with updates including the Indonesian Throughflow (assumed to be 10 Sv at 24°C) and replacing the section south of New Zealand with the SR3 section south of Australia. Also shown are results from the recent inverse models of *Macdonald* [1998], *Sloyan and Rintoul* [2000a,b], and *Ganachuad* [1999].

in the meridional heat flux in the Indian and Pacific subtropical basins; changes in the air-sea heat flux; or changes in the heat transport carried by the barotropic flow. We are not yet able to determine which combination of these factors is at work, but the magnitude of the heat transport variations suggests the possibility of significant climate feedbacks.

Also of interest are the links between changes in transport of individual density layers (Plate 2) and the large-scale interbasin circulations. The transport changes at depth are small ($< \pm 2$ Sv). The largest transport changes occur in the light layers at the northern end of the section (SAMW and lighter layers), whose transport varies between about 9 and 17 Sv. The inverse model of *Sloyan and Rintoul* [2000a] shows that the SAMW participates in a circum-Australia circulation in the upper layers of the Indian and Pacific basins, as follows: more SAMW enters the Pacific across SR3 than leaves through Drake Passage; the excess SAMW feeds the northward flow, which (after substantial water mass modifications) ultimately supplies the Indonesian throughflow; throughflow water crosses the Indian basin and is carried south in the Agulhas Current; cooling and freshening over the Agulhas extension converts warm thermocline water supplied by the throughflow to SAMW; and part of the SAMW formed in the Indian sector is exported back to the Pacific across SR3 to close the loop. Variations in the export of SAMW to the Pacific across SR3 may be compensated by changes in storage, or by changes along this circuitous flow path. On the basis of repeats of a single section we can only identify this intriguing mode of interannual oceanic variability. Further studies with the complete WOCE data set will provide additional insight into the impact of the variations found on SR3. In this regard it is of interest that when the inverse model of *Sloyan and Rintoul* [2000a] is run with different realizations of SR3, the largest change in the solution is an increase or decrease in the strength of the Indonesian Throughflow and a compensating change in the transport of SAMW at SR3.

5. Conclusions

We have described the major circulation features south of Australia and quantified the baroclinic transport variability on the basis of six occupations of the WOCE SR3 section near 140°E (Figure 6). The mean top-to-bottom baroclinic transport (relative to a best guess reference level discussed in section 3.2) is 147 ± 10 Sv. The transport of the individual fronts of the ACC is remarkably steady with time. Variations in the net transport of mass and heat across SR3 are linked to variations in the westward flow of relatively warm water across the northern end of the section. While it is true that the ACC is the primary means by which water is exchanged between basins, the variability in interbasin exchange south of Australia is dominated by changes in flow north of the ACC. While the number of sections is small, the strength of the westward flow (and hence the net heat flux across the section) appears to be correlated with meridional shifts of the wind stress curl pattern. In density layers the deep flow is similar on each of the six occupations, but there are significant changes in the transport of the SAMW density class.

The mean (baroclinic) transport across SR3 is about 13 Sv larger than the present best estimate of the mean absolute transport through Drake Passage. The difference between the transport entering the Pacific south of Australia and that leaving the basin south of America is of the right order to balance the outflow from the Pacific through Indonesia and the Bering Strait. However, given the uncertainty in the barotropic transport at both locations, the agreement is likely fortuitous.

We have used the repeat measurements at SR3 to update estimates of interbasin exchange between the Indian and Pacific, following the lead of *Georgi and Toole* [1982]. Taking into account an Indonesian Throughflow of 10 Sv with a transport-weighted temperature of 24°C, the Pacific as a whole is found to gain heat (0.7 PW) while the Indian and Atlantic basins lose heat (-0.4 and -0.3 PW, respectively). Including the Indonesian Throughflow reverses the sign of the net heat exchange in the Indian and Pacific basins inferred by *Georgi and Toole* [1982].

One justification for repeat hydrography during WOCE was the need to assess the representativeness of the WOCE "one-time" survey. The observed range in eastward heat flux across SR3 is large relative to the meridional transport of heat in the Southern Hemisphere subtropical gyres. On the basis of a single repeat section it is not possible to determine the impact of these heat and volume transport anomalies on basin heat budgets or regional climate. The basin-wide synthesis of WOCE observations will provide some insight, although accounting for variability such as that observed on SR3 presents one of the more formidable and important challenges to such analyses. An expanded array of sustained, broad-scale oceanographic observations (e.g., from profiling floats), additional repeat sections, and direct measurements of ocean currents are also needed to determine the climate significance of the variability observed in the Southern Ocean.

Acknowledgments. We thank the officers and crew of the RSV *Aurora Australis* for their contributions to this work. Mark Rosenberg ensured the high quality of the CTD data. John Church played an important role in securing support for this program. Nathan Bindoff acted as Principal Investigator on two of the SR3 transects. Russ Davis supplied the ALACE floats and provided the data prior to publication. We thank John Toole for his contribution to the discussion of interbasin exchange. Karen Heywood and an anonymous reviewer provided many useful suggestions that helped improve the manuscript. The support of the Australian National Antarctic Research Expeditions (ANARE) and Environment Australia through the National Greenhouse Research Program is gratefully acknowledged. This paper is a contribution to the World Ocean Circulation Experiment.

References

Bindoff, N. L., M. J. Warner, and M. A. Rosenberg, On the circulation of the waters over the Antarctic continental

slope and rise between 80° and 150°E, *Deep Sea Res., Part II, 47*, 2299–2326, 2000.

Botnikov, V. N., Geographical position of the Antarctic convergence zone in the Pacific Ocean, *Sov. Antarct. Exped. Inf. Bull., Engl. Trans., 4*, 324–327, 1963.

Broecker, W. J., The great ocean conveyor, *Oceanography, 4*, 79–89, 1991.

Coachman, L., and K. Aagaard, Transports through Bering Strait: Annual and interannual variability, *J. Geophys. Res., 93*, 15,535–15,539, 1988.

Cresswell, G. R., A. Frische, J. Peterson, and D. Quadfasel, Circulation in the Timor Sea, *J. Geophys. Res., 98*, 14,379–14,389, 1993.

Davis, R. E., Preliminary results from directly measuring middepth circulation in the tropical and South Pacific, *J. Geophys. Res., 103*, 24,619–24,639, 1998.

Davis, R. E., D. C. Webb, L. A. Regier, and J. Dufour, The autonomous Lagrangian circulation explorer (ALACE), *J. Atmos. Oceanic Technol., 9*, 264–285, 1992.

De Ruijter, W. P. M., and D. B. Boudra, The wind-driven circulation in the South Atlantic-Indian Ocean, I, Numerical experiments in a one-layer model, *Deep Sea Res., Part A, 32*, 557–574, 1985.

Fahrbach, E., G. Rohardt, M. Schroder, and V. Strass, Transport and structure of the Weddell Gyre, *Ann. Geophys., 12*, 840–855, 1994.

Ganachaud, A. S., Large scale oceanic circulation and fluxes of freshwater, heat, nutrients and oxygen, Ph.D. thesis, Mass. Inst. of Tech. - Woods Hole Oceanog. Inst. Joint Program, Cambridge, 1999.

Georgi, D. T., and J. M. Toole, The Antarctic Circumpolar Current and the oceanic heat and freshwater budgets, *J. Mar. Res., 40* suppl., 183–197, 1982.

Gordon, A. L., Interocean exchange of thermocline water, *J. Geophys. Res., 91*, 5037–5046, 1986.

Gordon, A. L., and E. J. Molinelli, *Southern Ocean Atlas*, 200 pp., Columbia Univ. Press, New York, 1982.

Gouretski, V., and K. Jancke, A new world ocean climatology: Objective analysis on neutral surfaces, *WOCE Rep. 256/17*, World Ocean Circ. Exp. Hydrogr. Prog. Spec. Anal. Cent., Hamburg, Germany, 1998.

Heil, P., and I. Allison, The pattern and variability of Antarctic sea-ice drift in the Indian Ocean and western Pacific sectors, *J. Geophys. Res., 104*, 15,789–15,802, 1999.

Heywood, K. J., M. D. Sparrow, J. Brown, and R. R. Dickson, Frontal structure and Antarctic Bottom Water Flow through the Princess Elizabeth Trough, Antarctica, *Deep Sea Res., Part I, 46*, 1181–1200, 1999.

Jackett, D. R., and T. J. McDougall, A neutral density variable for the World's Oceans, *J. Phys. Oceanogr., 27*, 237–263, 1997.

Jacobs, S. S., On the nature and significance of the Antarctic Slope Front, *Mar. Chem., 35*, 9–24, 1991.

Kalnay, E., and et al., The NCEP/NCAR 40-year reanalysis project, *Bull. Am. Meteorol. Soc., 77*, 347–471, 1996.

Macdonald, A. M., The global ocean circulation: A hydrographic estimate and regional analysis, *Prog. Oceanog., 41*, 281–382, 1998.

Meyers, G., R. J. Bailey, and A. P. Worby, Geostrophic transport of Indonesian throughflow, *Deep Sea Res., Part I, 42*, 1163–1174, 1995.

Nowlin, W. D. J., and M. Clifford, The kinematic and thermohaline zonation of the Antarctic Circumpolar Current at Drake Passage, *J. Mar. Res., 40* suppl., 481–507, 1982.

Orsi, A. H., T. W. Whitworth III, and W. D. Nowlin Jr., On the meridional extent and fronts of the Antarctic Circumpolar Current, *Deep Sea Res., Part I, 42*, 641–673, 1995.

Peterson, R. G., On the transport of the Antarctic Circumpolar Current through Drake Passage and its relation to wind, *J. Geophys. Res., 93*, 13,993–14,004, 1988.

Reid, J., and W. D. Nowlin Jr., Transport of water through Drake Passage, *Deep-Sea Res. Oceanog. Abstr., 18*, 51–64, 1971.

Rintoul, S. R., On the origin and influence of Adelie Land Bottom Water, in *Ocean, Ice and Atmosphere: Interactions at the Antarctic Continental Margin, Ant. Res. Ser.*, vol. 75, edited by S. S. Jacobs, and R. Weiss, pp. 151–171, AGU, Washington, D.C., 1998.

Rintoul, S. R., and J. L. Bullister, A late winter hydrographic section from Tasmania to Antarctica, *Deep Sea Res., Part I, 46*, 1417–1454, 1999.

Rintoul, S. R., J.-R. Donguy, and D. H. Roemmich, Seasonal evolution of upper ocean thermal structure between Tasmania and Antarctica, *Deep Sea Res., Part I, 44*, 1185–1202, 1997.

Robbins, P. E., and J. M. Toole, The dissolved silica budget as a constraint on the meridional overturning circulation of the Indian Ocean, *Deep Sea Res., Part I, 44*, 879–906, 1997.

Rosenberg, M., R. Eriksen, and S. Rintoul, Aurora Australis marine science cruise AU9309/AU9391: Oceanographic field measurements and analysis, *Res. Rep. 2*, 103 pp., Antarct. Coop. Res. Cent., Hobart, Tasmania, Australia, 1995a.

Rosenberg, M., R. Eriksen, S. Bell, N. Bindoff, and S. Rintoul, Aurora Australis marine science cruise AU9407: Oceanographic field measurements and analysis, *Res. Rep. 6*, 97 pp., Antarct. Coop. Res. Cent., Hobart, Tasmania, Australia, 1995b.

Rosenberg, M., R. Eriksen, S. Bell, and S. Rintoul, Aurora Australis marine science cruise AU9404: Oceanographic field measurements and analysis, *Res. Rep. 8*, 53 pp., Antarct. Coop. Res. Cent., Hobart, Tasmania Australia, 1996.

Rosenberg, M., S. Bray, N. Bindoff, S. Rintoul, N. Johnson, S. Bell, and P. Towler, Aurora Australis marine science cruise AU9501, AU9604, and AU9601: Oceanographic field measurements and analysis, inter-cruise comparisons and data quality notes, *Res. Rep. 12*, 150 pp., Antarct. Coop. Res. Cent., Hobart, Tasmania, Australia, 1997.

Schodlock, M. P., M. Tomczak, and N. White, Deep sections through the South Australian Basin and across the Australian–Antarctic Discordance, *Geophys. Res. Lett., 24*, 2785–2788, 1997.

Sloyan, B. M., and S. R. Rintoul, Circulation, renewal and modification of Antarctic mode and intermediate water, *J. Phys. Oceanogr.*, in press, 2000a.

Sloyan, B. M., and S. R. Rintoul, The Southern Ocean limb of the global deep overturning circulation, *J. Phys. Oceanogr.*, in press, 2000b.

Sokolov, S., and S. R. Rintoul, Some remarks on interpolation of nonstationary oceanographic fields, *J. Atmos. Oceanic Technol., 16*, 1434–1449, 1999.

Sokolov, S., and S. R. Rintoul, Circulation and water masses along WOCE section P11: Papua New Guinea to Tasmania, *J. Mar. Res., 58*, 223–268, 2000.

Tchernia, P., and P. F. Jeannin, Quelques aspects de la circulation oceanique Antarctique reveles par l'observation de la derive d'icebergs, *Rep. 3*, 92 pp., Cent. Natl. d'Etud. Spatiales, Mus. Nat. Hist. Nat., Paris, 1983.

Toole, J. M., and B. Warren, A hydrographic section across the subtropical South Indian Ocean, *Deep Sea Res., Part I, 40*, 1973–2019, 1993.

White, W. B., and N. J. Cherry, Influence of the Antarctic Circumpolar Wave upon New Zealand temperature and precipitation during autumn-winter, *J. Clim., 12*, 960–976, 1998.

White, W. B., and R. Peterson, An Antarctic Circumpolar

Wave in surface pressure, wind, temperature and sea ice extent, *Nature*, *380*, 699–702, 1996.

Whitworth, T., III, Zonation and geostrophic flow of the Antarctic Circumpolar Current at Drake Passage, *Deep Sea Res., Part A*, *27*, 497–507, 1980.

Whitworth, T., III, Monitoring the net transport of the Antarctic Circumpolar Current at Drake Passage, *J. Phys. Oceanogr.*, *13*, 2045–2057, 1983.

Whitworth, T., III, and R. G. Peterson, The volume transport of the Antarctic Circumpolar Current from three-year bottom pressure measurements, *J. Phys. Oceanogr.*, *15*, 810–816, 1985.

Whitworth, T., III, W. D. Nowlin Jr., and S. J. Worley, The net transport of the Antarctic Circumpolar Current through Drake Passage, *J. Phys. Oceanogr.*, *12*, 960–971, 1982.

Whitworth, T., III, A. H. Orsi, S.-J. Kim, W. D. Nowlin Jr., and R. A. Locarnini, Water masses and mixing near the Antarctic Slope Front, in *Ocean, Ice and Atmosphere: Interactions at the Antarctic Continental Margin, Ant. Res. Ser.*, vol. 75, edited by S. S. Jacobs, and R. Weiss, pp. 1–27, AGU, Washington, D.C., 1998.

Wyrtki, K., The flow of water into the deep sea basins of the western South Pacific Ocean, *Aust. J. Mar. Freshwater Res.*, *12*, 1–16, 1961.

Wyrtki, K., The subsurface water masses in the western South Pacific Ocean, *Aust. J. Mar. Freshwater Res.*, *13*, 18–47, 1962.

Yaremchuk, M. I., N. L. Bindoff, J. Schröter, D. Nechaev, and S. R. Rintoul, On the zonal and meridional circulation and ocean transports between Tasmania and Antarctica, *J. Geophys. Res.*, this issue.

S. R. Rintoul and S. Sokolov, CSIRO Marine Research and Antarctic Cooperative Research Centre, GPO Box 1538, Hobart, Tasmania 7001, Australia. (steve.rintoul@marine.csiro.au)

(Received July 15, 1999; revised April 19, 2000; accepted June 12, 2000.)